Journal of Solid State Chemistry 182 (2009) 630–639

Contents lists available at ScienceDirect

Journal of Solid State Chemistry

journal homepage: www.elsevier.com/locate/jssc

Sn_4As_3 revisited: Solvothermal synthesis and crystal and electronic structure

Kirill Kovnir [a,*], Yury V. Kolen'ko [b,1], Alexey I. Baranov [a,2], Inés S. Neira [b], Alexey V. Sobolev [c], Masahiro Yoshimura [b], Igor A. Presniakov [c], Andrei V. Shevelkov [c]

[a] *Department of Materials Science, Lomonosov Moscow State University, 119991 Moscow, Russia*
[b] *Materials and Structures Laboratory, Tokyo Institute of Technology, 4259 Nagatsuta, Midori-ku, Yokohama 226-8503, Japan*
[c] *Chemistry Department, Lomonosov Moscow State University, 119991 Moscow, Russia*

ARTICLE INFO

Article history:
Received 3 October 2008
Received in revised form
11 December 2008
Accepted 13 December 2008
Available online 24 December 2008

Keywords:
Tin arsenide
Sn_4As_3
Solvothermal synthesis
Quantum-chemical calculations
Electronic structure
ELF
Lone pair
Mössbauer spectroscopy

ABSTRACT

A facile one pot method of synthesis of tin arsenide Sn_4As_3 starting from metallic tin and elemental arsenic under mild solvothermal conditions in ethylenediamine in the presence of ammonium chloride is offered. The dissolving of the tin metal in ethylenediamine and the role of NH_4Cl are discussed. The crystal structure of Sn_4As_3 has been re-determined. It is shown to crystallize in the trigonal non-centrosymmetric space group $R3m$, ($a = 4.089(1)$ Å, $c = 36.059(6)$ Å, $Z = 3$), which differs from the previously reported centrosymmetric structure ($R\bar{3}m$). The crystal structure of Sn_4As_3 consists of alternating layers of arsenic and tin atoms that are combined into seven-layer blocks and build up along the *c*-axis. The major structural feature is the short tin–tin distances (3.24 Å) between the adjacent blocks. The analysis of the density of states and band structure reveals that Sn_4As_3 should have metallic properties, which is in line with the previously reported experimental observations. Analysis of chemical bonding employing the electron localization function shows that only for the shortest Sn–As contacts the bonding is pairwise, while four-center bonds are formed between arsenic and tin atoms at relatively long distances (>2.85 Å). Moreover, each tin atom holds an electron lone-pair.

1. Introduction

Metal pnictides, being widely explored in semiconductor technology [1], are also promising systems for the development of thermoelectric materials [2], negative electrode materials for Li-ion batteries [3], functional catalysts [4], solar cells [5], and fast thermal detectors [6]. Pnictides chemistry and physics have gained the fundamental interest owing to the recent discovery of high temperature superconductivity ($T_C > 20$ K) in different ternary and quaternary iron arsenides [7]. The prospective technological applications demand the elaboration of the facile synthesis of these compounds as well as the exploration of their crystal and electronic structure and physical properties.

Various synthetic approaches towards metal arsenides are described in the literature. They include high temperature solid-state synthesis, high-pressure techniques, chemical transport reactions, metalorganic chemical vapor deposition, molecular beam epitaxy, as well as several solution methods [8,9]. The latter seem to be perspective for industrial applications since they require moderately low temperatures and can be scaled up. However, the reported approaches demand operations with hazardous and/or highly sensitive reagents, such as $AsCl_3$, As_2O_3, AsH_3, and Na_3As, which significantly limits the advantages of the solution-based syntheses. Therefore, a convenient and reliable synthesis of metal arsenides still remains a challenge.

Crystal structure, homogeneity range, and some properties of tin arsenide—Sn_4As_3—have been a matter of scientific discussion for last 80 years. The compound itself was first reported by Mansuri in 1923 [10], its crystal structure was determined by Hägg and Hybinette in 1935 [11], where a tin excess composition was assumed. In the late 60s, Eckerlin and Kischio [12] reported a tin-deficient crystal structure of $Sn_{4-\delta}As_3$, while the investigation of the Sn–As phase diagram by Peretti and Paulsen revealed a stoichiometric composition of Sn_4As_3 [13]. Six years later, Vdovina and Medvedeva re-investigated the tin–arsenic phase diagram and suggested that the Sn_4As_3 phase had a tin-rich homogeneity region ranging from 57 to 60 tin at.% [14]. Different transport properties were reported for variously prepared/treated samples, ranging from semiconducting [15] to metallic [12,15]. The superconductivity of Sn_4As_3 was reported at the temperature about several Kelvin [16]. All these discrepancies stimulated our detailed study of the synthesis, crystal and electronic structure of Sn_4As_3, which are reported in this manuscript.

---

[*] Corresponding author. Present address: Department of Chemistry and Biochemistry, Dittmer Bldg., Florida State University, 32306 Tallahassee, FL, USA. Fax: +1 850 644 8281.

E-mail address: kkovnir@chem.fsu.edu (K. Kovnir).

[1] Present address: Fritz Haber Institute of the Max Planck Society, 14195 Berlin, Germany.

[2] Present address: Max Planck Institute for Chemical Physics of Solids, 01187 Dresden, Germany.

0022-4596/$ - see front matter © 2008 Elsevier Inc. All rights reserved.
doi:10.1016/j.jssc.2008.12.007

2. Experimental

2.1. Solvothermal synthesis

Arsenic lump (98.0% Wako), tin metal powder (45 μm; 99.5% Wako), ethylenediamine (1,2-diaminoethane; 99.0% Wako), and ammonium chloride NH_4Cl (99.5% Wako) were used as received. Appropriate amounts (Table 1) of elemental arsenic (thoroughly reground) and tin together with NH_4Cl were mixed with 35 cm^3 of ethylenediamine in a 40 cm^3 poly(tetrafluoroethylene) (PTFE) vessel; the vessel was then capped by a PTFE cover and placed inside a stainless steel bomb. The bomb was sealed and kept at required temperature (473–513 K) for the desired period of time (20–120 h). The product of the solvothermal process was collected by filtration, washed with distilled water and ethanol, and then dried in a moisture-free desiccator. To remove the admixtures of metallic tin and tin oxide from the as-prepared samples, a washing of the product was carried under vigorous stirring in 0.01 M HCl aqueous solution for 3 h. Throughout this work, a set of acronyms is used (Table 1). The first two letters mean the desired Tin Arsenide (TA), and the number of the sample follows.

2.2. Solid-state synthesis

Elemental tin (Reakhim, 99.99%) and arsenic (Reakhim, 99.99%) were used as starting materials. The stoichiometric molar ratio (4:3) of the reagents was utilized. Synthesis was performed in a silica tube sealed under vacuum, residual pressure 10^{-2} mbar (length: 60 mm; inner diameter: 8 mm). The sample was annealed at 723 K for 5 days (heating rate: 0.6 K/min) and then cooled in a furnace. After regrinding, the sample was sealed in the silica tube of the same dimensions, annealed at 723 K for additional 5 days, and then quenched in the ice water bath, which resulted in a single-phase product. A single crystal for the X-ray diffraction experiment was selected from the sample after the first annealing. All our attempts to obtain single phase product by slow cooling of the Sn–As melt failed.

2.3. Characterization

The products of the syntheses were characterized by means of powder X-ray diffraction (XRD) using either a Rigaku RINT 2000 diffractometer with Ni-filtered Cu$K\alpha$ radiation ($\lambda = 1.54178$ Å) or Huber G670 Image Plate Camera, Cu$K\alpha_1$ ($\lambda = 1.540598$ Å). The unit cell parameters were refined by least-square fits of diffraction peak positions of the main phase in the hexagonal system in the $R3m$ space group using LaB_6 ($a = 4.15692$ Å) as an internal standard and employing WinCSD software [17]. In order to estimate relative amounts of admixtures, the Rietveld refinement was carried out utilizing JANA2000 software [18]. The morphology was studied by scanning electron microscopy (SEM) using a Hitachi S-4500 microscope operating at 15 kV.

2.4. Single crystal X-ray diffraction experiment

A selected single crystal was mounted on a goniometer head of a CAD-4 (Nonius) diffractometer. The orientation matrix was refined on the basis of 24 well-centered reflections in the angular range of $16^\circ < \theta < 19^\circ$, and the corresponding unit cell parameters agreed well with those found from the powder diffraction data. The SHELX-97 programs were used for the crystal structure solution and refinement [19]. Details of the X-ray diffraction experiments are presented in Table 2, while the atomic coordinates and selected interatomic distances are listed in Tables 3 and 4, respectively.

2.5. Mössbauer spectroscopy

The ^{119}Sn spectrum was recorded using a conventional constant acceleration Mössbauer spectrometer MS1104E. The measurements were performed at 300 K with the Ca^{119m}SnO$_3$ source maintained at room temperature. Isomer chemical shifts are referenced to a $CaSnO_3$ absorber at 300 K.

2.6. Quantum chemical calculations

Electronic structure calculations and bonding analysis for Sn_4As_3 were carried out using the tight binding-linear muffin tin orbitals-atomic sphere approximation (TB-LMTO-ASA) program package [20]. The von Barth–Hedin exchange-correlation potential [21] was employed for the local density approximation (LDA) calculations. The radial scalar-relativistic Dirac equation was solved to obtain the partial waves. Since the calculation within the ASA should include corrections for the neglect of interstitial regions and partial waves of higher order [22], 16 empty spheres of seven different radii were added to the structure. The following radii of the atomic spheres were applied for the calculations for Sn_4As_3: $r(\text{Sn1}) = 1.73$ Å, $r(\text{Sn2}) = 1.68$ Å, $r(\text{Sn3}) = 1.68$ Å, $r(\text{Sn4}) = 1.65$ Å, $r(\text{As1}) = 1.55$ Å, $r(\text{As2}) = 1.60$ Å, and $r(\text{As3}) = 1.55$. A basis set containing Sn(5s,5p) and As(4s,4p) orbitals was employed for a self-consistent calculation, with Sn(5d,4f) and As(4d) functions being downfolded. The electron localization function (ELF), η, [23]

Table 1
Summary of the selected reactions resulting in the formation of Sn_4As_3 as a main product.

Sample	Sn:As	Synthesis conditions[a]	Admixtures wt.%[b] (Rietveld refinement)	Unit cell, $R3m$	
				a, Å	c, Å
TA-1	4:3	513 K, 40 h	SnAs: 3%; As: 3%	4.0903(1)	36.084(1)
TA-2	4.6:3	513 K, 40 h	SnAs: <1%; As: 1%; SnO: 5%	4.0904(1)	36.084(1)
TA-3	4.6:3	513 K, 60 h	SnAs: 1%; As: 1%; Sn: 3%	4.0904(1)	36.083(1)
TA-4	4.6:3	513 K, 80 h	SnAs: 1%; As: 1.5%	4.0903(1)	36.086(1)
TA-5	5.2:3	513 K, 80 h	SnAs: <1%; As: 1%; Sn: 3%; SnO: 1%	4.0906(1)	36.083(1)
TA-5w	Washing[c]		As: 5%	4.0902(1)	36.084(1)
TA-6	5.2:3	513 K, 120 h	SnAs: <1%; As: <1%	4.0901(1)	36.083(1)
TA-7	Solid state synthesis		None	4.0901(2)	36.072(2)

Solvothermal reactions were performed in 35 cm^3 of ethylenediamine starting from 14 mmol NH_4Cl, 3.75 mmol of As and appropriate amounts of Sn powder.

[a] Syntheses at 473 K resulted in a relatively high amount (~10 mol.%) of non-reacted Sn and As in the products.

[b] No traces of ammonium chloride were found in the products.

[c] **TA-5** washed in 0.01 M HCl.

was evaluated with modules implemented within the TB-LMTO-ASA program package [20]. The Data Explorer program was used for visualization of ELF isosurfaces [24]. Additionally, hypothetical structures of Sn_4As_3 were calculated. In such models the symmetry of unit cell and the structure of seven-layer blocks were kept alike to Sn_4As_3, while the inter-block separation was artificially increased together with elongation of the unit cell in the [0001] direction.

Table 2
Data collection and structure refinement parameters for Sn_4As_3[a].

Composition	Sn_4As_3
Space group	$R3m$ (no. 160)
Temperature (K)	293(2)
Cell parameter	
a (Å)	4.089(1)
c (Å)	36.059(6)
V (Å^3)	522.1(2)
Z	3
Density (calc.) (g cm^{-3})	6.674
μ (mm^{-1})	28.211
Data collection range (deg)	$3.4<\theta<28.9$
Reflections collected	1308
Independent reflections	442 [$R_{int}=0.107$]
Parameters refined	23
R_1[b]	0.039
wR_2[c] [$F_o>4\sigma F_o$]	0.093
R_1	0.041
wR_2 (all data)	0.103
Flack parameter of absolute structure	0.0(1)
Largest diff. peak and hole (e/Å^3)	1.32 and −1.41
Goodness-of-fit	1.176

[a] Further details of the crystal structure determination may be obtained from Fachinformationszentrum Karlsruhe, D-76344 Eggenstein-Leopoldshafen, Germany, on quoting the depository number CSD-419884.

[b] $R_1=\Sigma\|F_o|-|F_c\|/\Sigma|F_o\|$.

[c] $wR_2=[\Sigma w(F_o^2-F_c^2)^2/\Sigma w(F_o^2)^2]^{1/2}$, $w=[\sigma^2(F_o^2)+(Ap)^2+Bp]^{-1}$; $p=(F_o^2+2F_c^2)/3$; $A=0.0473$, $B=0.746$.

Table 3
Atomic coordinates and equivalent displacement parameters for Sn_4As_3.

Atom	Site	x/a	y/b	z/c	U_{eq}[a]
Sn(1)	3m	0	0	0.2907(1)	0.016(1)
Sn(2)	3m	0	0	0.7131(1)	0.015(1)
Sn(3)	3m	0	0	0.1378(1)	0.014(1)
Sn(4)	3m	0	0	0.8660(1)	0.014(1)
As(1)	3m	0	0	0.5724(2)	0.012(1)
As(2)	3m	0	0	0.0027(3)	0.012(1)
As(3)	3m	0	0	0.4323(2)	0.013(1)

[a] U_{eq} is defined as one third of the trace of the orthogonalized U_{ij} tensor.

3. Results and discussion

3.1. Solvothermal synthesis

Recently we have developed the solvothermal synthesis of tin phosphide, Sn_4P_3, starting from elemental tin and red phosphorus [25]. We have shown that the reaction between phosphorus dissolved in ethylenediamine and tin powder occurs at moderate temperature (473 K). Solvothermal syntheses of metal arsenides reported in the literature required operations with highly toxic/sensitive compounds: $AsCl_3$, As_2O_3, and $K(Na)BH_4$ [9]. Following the Sn_4P_3 trend and aiming at the development of a facile synthetic route to tin arsenide TA, we have chosen elemental tin and arsenic as starting materials:

$$4Sn+3As\rightarrow Sn_4As_3 \tag{1}$$

Unfortunately, no reaction was observed between As and Sn in ethylenediamine under solvothermal condition. Varying the solvent (EtOH, $NH_{3(aq)}$) allows us to perform the desired reaction in low yields; however, the process was accompanied by the oxidation of tin and arsenic resulting in significant amounts of oxides admixtures. To improve solubility of the starting materials in ethylenediamine, ammonium chloride was added, which resulted in formation of the desired phase in a high yield. The summary of selected solvothermal syntheses in ethylenediamine is given in Table 1.

The duration, temperature, as well as the initial components ratio were varied in the course of the reaction optimization. An increase of the reaction temperature leads to significantly higher yields of Sn_4As_3. It should be noted that our studies were limited by the melting temperature of a PTFE-cell used ($\leqslant$523 K). When the stoichiometric amounts of tin and arsenic are introduced into the reaction, the admixtures of arsenic and arsenic-rich tin arsenide SnAs are formed (**TA-1**). Using the 15 mol.% tin excess allowed us to diminish the arsenic-containing admixtures, but higher reaction time was necessary to avoid non-reacted tin or tin oxide in the products (**TA-2**>**TA-3**>**TA-4**). The syntheses started from the 30 mol.% tin excess required further increasing of reaction time up to 120 h; however, even in the case of the sample **TA-6**, a complete elimination of arsenic admixtures was not achieved. Decreasing the ammonium chloride amounts led to

Table 4
Selected interatomic distances (Å) and angles (°) in the crystal structure of Sn_4As_3.

Atoms	Distance	Atoms	Angle	Atoms	Angle
Sn(1)–As(1)	3.006(7) × 3	As(2)–Sn(1)–As(2)	90.8(3) × 3	Sn(4)–As(1)–Sn(4)	95.6(2) × 3
Sn(1)–As(2)	2.872(7) × 3	As(2)–Sn(1)–As(1)	176.5(3) × 3	Sn(4)–As(1)–Sn(1)	173.0(3) × 3
Sn(2)–As(2)	2.839(7) × 3	As(2)–Sn(1)–As(1)	91.7(1) × 6	Sn(4)–As(1)–Sn(1)	89.15(6) × 6
Sn(2)–As(3)	3.029(6) × 3	As(1)–Sn(1)–As(1)	85.7(2) × 3	Sn(1)–As(1)–Sn(1)	85.7(2) × 3
Sn(3)–As(3)	2.743(4) × 3	As(2)–Sn(2)–As(2)	92.1(3) × 3	Sn(2)–As(2)–Sn(2)	92.1(3) × 3
Sn(3)–Sn(4)	3.242(1) × 3	As(2)–Sn(2)–As(3)	175.0(3) × 3	Sn(2)–As(2)–Sn(1)	179.0(4) × 3
Sn(4)–As(1)	2.760(4) × 3	As(2)–Sn(2)–As(3)	91.4(1) × 6	Sn(2)–As(2)–Sn(1)	88.55(2) × 6
Sn(4)–Sn(3)	3.242(1) × 3	As(3)–Sn(2)–As(3)	84.9(2) × 3	Sn(1)–As(2)–Sn(1)	90.8(3) × 3
As(1)–Sn(1)	3.006(7) × 3	As(3)–Sn(3)–As(3)	96.4(1) × 3	Sn(3)–As(3)–Sn(3)	96.4(1) × 3
As(1)–Sn(4)	2.760(4) × 3	As(3)–Sn(3)–Sn(4)	167.4(1) × 3	Sn(3)–As(3)–Sn(2)	171.8(3) × 3
As(2)–Sn(1)	2.872(7) × 3	As(3)–Sn(3)–Sn(4)	92.0(1) × 6	Sn(3)–As(3)–Sn(2)	89.06(7) × 6
As(2)–Sn(2)	2.839(7) × 3	Sn(4)–Sn(3)–Sn(4)	78.21(4) × 3	Sn(2)–As(3)–Sn(2)	84.9(2) × 3
As(3)–Sn(2)	3.029(6) × 3	As(1)–Sn(4)–As(1)	95.6(2) × 3		
As(3)–Sn(3)	2.743(4) × 3	As(1)–Sn(4)–Sn(3)	168.0(1) × 3		
		As(1)–Sn(4)–Sn(3)	92.5(1) × 6		
		Sn(3)–Sn(4)–Sn(3)	78.21(4) × 3		

lower yields of the reaction while its increasing promoted a side reaction with the formation of SnAs.

By analogy to the Sn–P system [25], we applied the acidic washing in order to remove tin and tin oxide admixtures from the **TA-5** sample. As it turned out, tin arsenides are not stable against acidic treatment and even diluted HCl caused partial decomposition of Sn_4As_3 (**TA-5w**). The most pure sample (**TA-6**) was synthesized at 513 K starting from the tin to arsenic ratio 5.2:3. Despite the presence of minor admixtures of As and SnAs (less than 1 wt.% each) the achieved yield of the desired phase, Sn_4As_3, was very high ($>98\%$). According to SEM, the produced samples consisted of relatively big aggregates without any texturing, with the particles size ranging from several hundred nanometers to a few micrometers (Fig. 1).

Summarizing our synthetic results, we can conclude that the probable mechanism of the solvothermal reaction is different for Sn_4P_3 and Sn_4As_3. In the former case, phosphorus is a component which dissolves in ethylendiamine, and equilibrium is achieved between the solid metal, dissolved phosphorus, and metal phosphide. Significant excess of phosphorus is required to shift the equilibrium position towards the formation of the metal phosphide [25]. However, ethylenediamine itself is able to dissolve neither elemental tin nor arsenic.

When ammonium chloride is added to the ethylenediamine, it dissociates to an acid–base couple of NH_4^+ and Cl^-, which, in turn, leads to dissolution of tin instead of arsenic. Indeed, a requirement of tin excess as well as the presence of non-reacted arsenic point to this conclusion. In order to verify our assumption, a simple blank experiment was performed: 5 mmol of tin powder together with 14 mmol of NH_4Cl were mixed with 35 cm^3 of ethylenediamine in the PTFE vessel and the reaction was performed at 513 K for 10 h. After cooling down the remaining metallic tin was collected, washed to remove possible admixture of ammonium chloride and dried. The obtained tin yield was 95%, which means that 5% of elemental tin was dissolved in the ethylendiamine/NH_4Cl solution. This is direct evidence that metallic tin does dissolve in subcritical ethylenediamine (critical *T* of about 593 K) upon adding ammonium chloride. Thus, we have demonstrated that Sn_4As_3 can be synthesized in high yields utilizing simple and moisture stable reagents, such as elemental tin and arsenic together with ammonium chloride.

3.2. Crystal structure re-determination and description

The structure of Sn_4As_3 was determined by single-crystal X-ray diffraction method at ambient temperature (Table 2). The data set was indexed in the hexagonal unit cell with parameters $a = 4.089(1)$ Å and $c = 36.059(6)$ Å, which is in a good agreement with the powder diffraction data. No additional systematic extinctions, except those corresponding to the *R*-centered trigonal lattice [*hkil*], $-h+k+l = 3n$, were observed. For the structure refinement, the proposed in the literature [11,12] model in the $R\bar{3}m$ (no. 166) space group, was taken. The final refinement within this model with anisotropic atomic displacement parameters for all atoms ($R_1 = 0.051$) reveals presence of high difference peaks (4–6 e/Å^3) close to both tin and one arsenic atoms, indicating possible splitting of the atomic positions. At the second stage, the refinement was performed in the non-centrosymmetric space group $R3m$ (no. 160), which results in the removal of splitting of all atomic positions and in considerable decreasing of *R* values. Such a transformation resulted in the relative displacement of the previously equivalent tin and arsenic atoms by 0.1–0.2 Å along the *c*-axis as well as the shift of the arsenic atom from the origin of the unit cell by 0.1 Å. Since the significant homogeneity range was previously reported for Sn_4As_3 [11–14], the occupancy values were allowed to vary in a separate series of the least-squares refinement. The resulting occupancies turned out to be equal to unity within three e.s.d., confirming the 4:3 tin to arsenic ratio for the investigated crystal. In the final refinement series, full occupancies were assumed for all positions. The final refinement

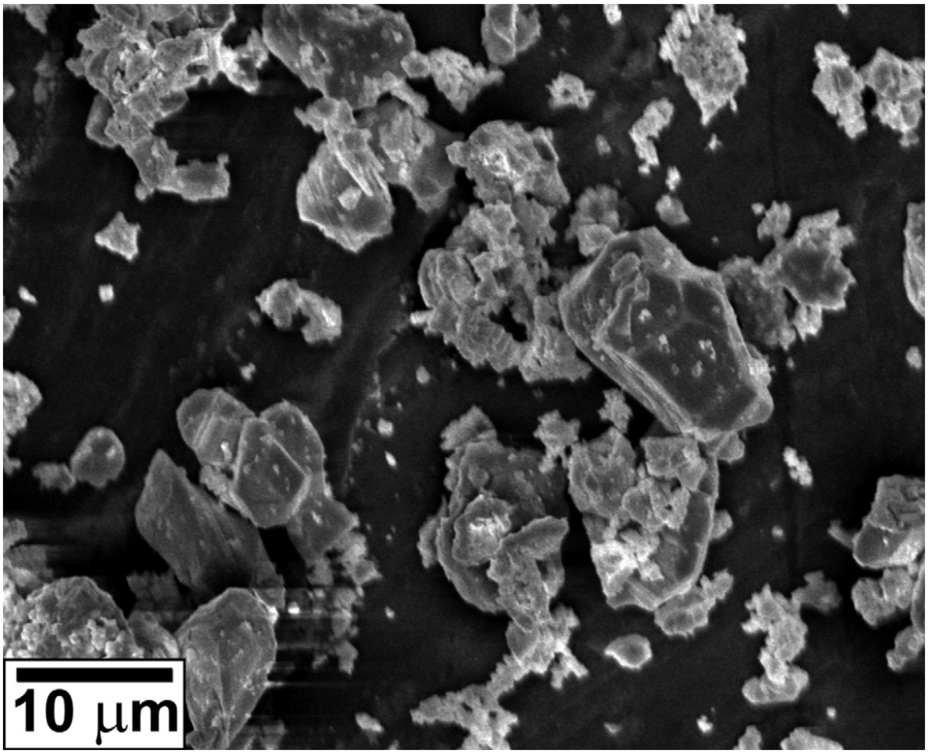

Fig. 1. SEM microphotograph of the solvothermally derived polycrystalline Sn_4As_3 (**TA-6**).

in the $R3m$ space group with anisotropic atomic displacement parameters for all atoms converged to $R_1 = 0.039$.

The crystal structure of Sn_4As_3 (Fig. 2) consists of alternating layers of arsenic and tin atoms that are combined into seven-layer blocks that build up along the c-axis. There are two types of tin atom coordination in the crystal structure. The Sn(1) and Sn(2) atoms are octahedrally coordinated by arsenic atoms only (2.84–3.03 Å) and do not form any Sn—Sn bonds (Fig. 3). The Sn(3) and Sn(4) atoms, confining the block, have a [3+3] coordination composed by three arsenic atoms from one side (2.74–2.76 Å) and three tin atoms of the other type, Sn(4) or Sn(3), respectively, from the adjacent block at a relatively long distance of 3.24 Å. The arsenic atoms are always surrounded by six tin atoms forming slightly (As(2)) or strongly distorted (As(1) and As(3)) octahedra (Fig. 3 and Table 4). Such a kind of coordination is not typical for arsenic which prefers to be tetrahedrally coordinated by metals in most arsenides. Within each block, there is one layer of atoms of each type such that the layer of arsenic atoms separates the layers of tin atoms (Fig. 2).

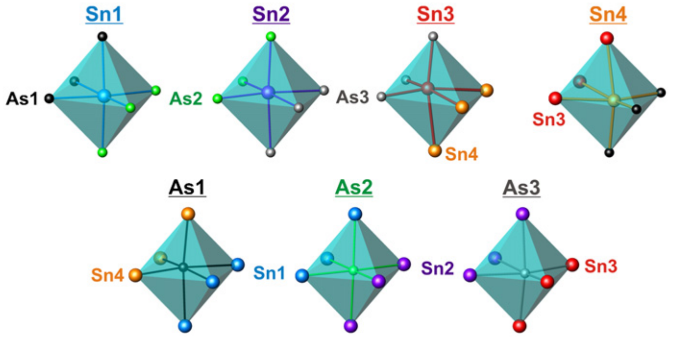

Fig. 3. Coordination of the atoms in the crystal structure of Sn_4As_3.

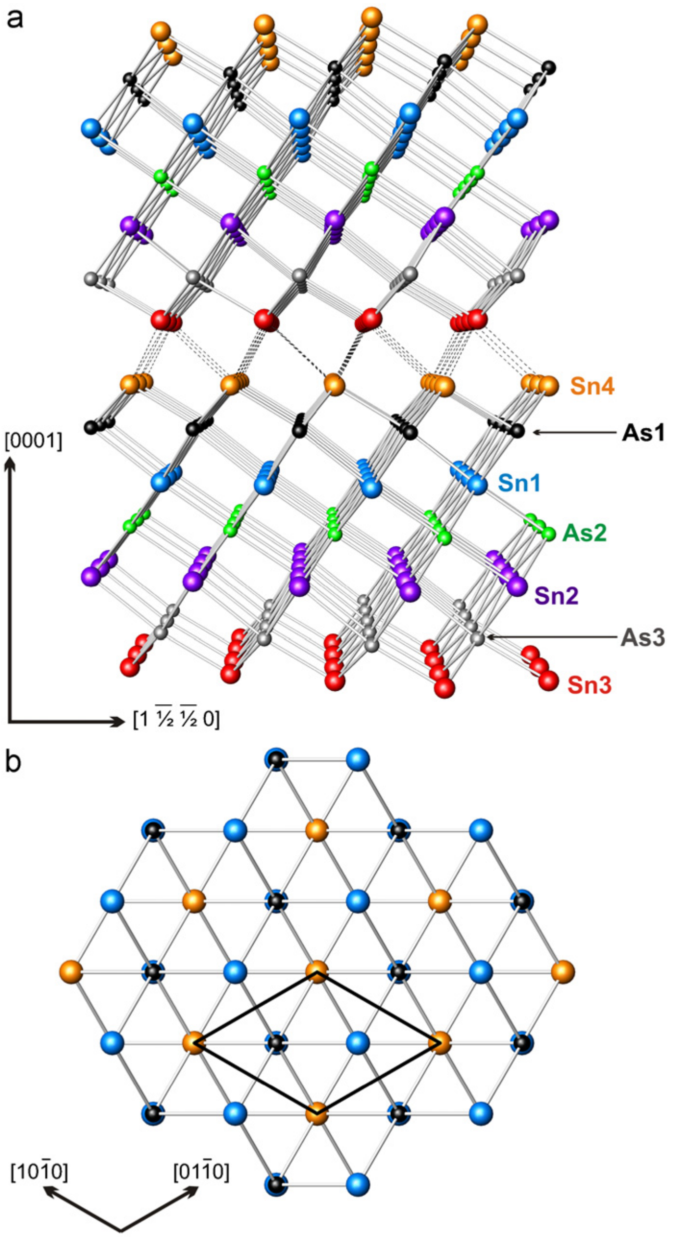

Fig. 2. Crystal structure of Sn_4As_3: (a) view of two adjacent seven-layer blocks of tin and arsenic atoms, long Sn–Sn distances are shown by dashed lines; (b) projection on the [0 0 0 1].

The crystal structure of Sn_4As_3 is closely related to the structure of tin phosphide Sn_4P_3 while having an important difference—the absence of the inversion center. Sn_4P_3 has a similar structure consisting of the seven-layer blocks of tin and phosphorus atoms, with Sn–Sn distances between the blocks of 3.25 Å. However, Sn_4P_3 crystallizes in the centrosymmetric space group $R\bar{3}m$ (no. 166) [14,26] and its unit cell contains only four symmetrically non-equivalent atoms; they are two tin and two arsenic atoms. Exactly the same centrosymmetric structure was proposed for Sn_4As_3 in the literature [11,12]. In the case of Sn_4As_3 our data clearly point to the non-centrosymmetric group $R3m$ (no. 160). In the centrosymmetric space group pairs of the atoms Sn(1) and Sn(2); Sn(3) and Sn(4); As(1) and As(3) would become symmetrically equivalent, while in the actual crystal structure each atom of these couples has slightly different coordinates and environment (Tables 3 and 4).

The tin–arsenic distances in Sn_4As_3 are significantly elongated compared to other metal arsenides. In covalent $MSnAs_2$ ($M =$ Zn, Cd) compounds, tin atoms are tetrahedrally coordinated by four arsenic atoms at distances of 2.55–2.58 Å [27]. Longer tin–arsenic distances (2.60–2.78 Å) were reported for Zintl phases, wherein a tin–arsenic anion is supposed to carry a negative charge [28]. Significantly longer tin–arsenic distances were found for cationic Sn–As frameworks in inverse clathrates: 2.49–3.11 Å [29]. In Sn_4As_3, most of the Sn–As distances exceed the range reported for Zintl phases, but are similar to long distances in inverse clathrates (Table 4).

The crystal structure of Sn_4As_3 can be described as layered only in the case when the Sn–Sn interaction between two adjacent blocks is neglected. It may seem reasonable for tin phosphides with relatively long Sn–Sn distances between layers: Sn_3P_4 (d(Sn–Sn) = 3.38 Å) [2a] and SnP (d(Sn–Sn) = 3.48 Å) [30]. However, for Sn_4P_3 and the title tin arsenide, the distances of 3.24–3.25 Å appear to be too short to be disregarded. These distances are longer than those in elemental β-Sn (3.02 and 3.18 Å), but similar to the distances reported for binary strontium stannides, $SrSn_3$ and $SrSn_4$, ~3.3 Å [31]. The Sn–Sn distances within the range of 3.2–3.3 Å are longer than expected for localized Sn–Sn bonds, but rather are characteristic for delocalized bonding or lone pairs, as was shown by the ELF analysis [31,32]. The equally long tin–tin distances (3.2–3.3 Å) were reported for the three-dimensional frameworks of vacancy-containing clathrates $A_8Sn_{44}\square_2$ ($A =$ Cs, Rb; $\square =$ vacancy) [33] and $Sn_{24}P_{19.3}\square_{2.7}X_8$ ($X =$ I, Br) [34]. In the former case, tin atoms are coordinated by three tin atoms and one vacancy, while in the tin–phosphorus-halides part of the tin atoms has a [3+3] coordination, similar to the Sn(3) and Sn(4) atoms in Sn_4As_3. In order to estimate the properties of synthesized tin arsenide and to elucidate chemical bonding the detailed analysis of the electronic structure of Sn_4As_3 utilizing Mössbauer spectroscopy and quantum-chemical calculations was performed.

3.3. *Mössbauer spectroscopy*

The ^{119}Sn Mössbauer spectrum of Sn_4As_3 measured at 300 K is best fitted as a poorly resolved non-magnetic doublet (Fig. 4). To avoid complications with the fitting, the following constraints were applied. First, the two-doublet structure of the spectrum was derived from the crystal data, because the environments of Sn(1) and Sn(2) as well as of Sn(3) and Sn(4) are similar. Second, the areas (A) of the two doublets were fixed as 50% each since the amount of the atoms with the similar coordination is equal in the crystal structure. Finally, the half-width of the spectral components was constrained as equal. The resulting hyperfine parameters are given in Table 5. It is clear that the two doublets display rather close isomer shift (δ) and quadrupole splitting ($\varDelta$) values. To determine the factors governing the values of the δ and $\varDelta$ parameters, we performed calculations according to the semiempirical Townes–Daily model [35], which proved to be a useful tool for interpreting ^{119}Sn Mössbauer spectra of various tin derivatives [2a,29,36]. Within the frame of this model, the prevailing contribution of the Sn 5*p*-orbitals to the electric field gradient is assumed. In particular, the quadrupole splitting is described as

$$\varDelta = (e^2Q/2)U(1+\gamma^2/3)^{1/2} \tag{2}$$

where e is the electron charge, Q is the quadrupole constant for the ^{119}Sn nuclei, U is the parameter defining the deviation of the electron density from the spherical symmetry, and γ is the parameter defining the deviation of the electron density from the equatorial symmetry. The values of the U and γ parameters are connected with the distribution of the tin valence electrons such that

$$U = -N_z + \tfrac{1}{2}(N_x + N_y), \quad \gamma = (N_y - N_x)/N_z \tag{3}$$

where N_i ($i = x, y, z$) is the sum of the electronic populations along the respective direction. Application of these equations, using the crystal data and the $\varDelta$ value, enabled us to calculate the population of the lone electron pairs on the Sn(3) and Sn(4) atoms, directed from the respective atoms towards the triangle of three tin atoms from the neighboring block (Figs. 2 and 3). The population of the lone pair is estimated as 1.5 electrons, which indicates the incomplete localization of the lone pair on the respective tin atoms. For the given population of the lone pairs, the populations of the 5*s* and 5*p* orbitals of the Sn(3) and Sn(4) atoms were calculated to be 1.6 and 2.8, respectively. The obtained values were then used to calculate the value of the isomer shift [37]:

$$\delta_{\mathrm{sn}} = -0.433 + 3.01n_{5s} - 0.2n_{5s}^2 - 0.17n_{5s}n_{5p} \tag{4}$$

which leads to $\delta = 2.9\,\mathrm{mm\,s^{-1}}$, being in accordance with the value given in Table 5.

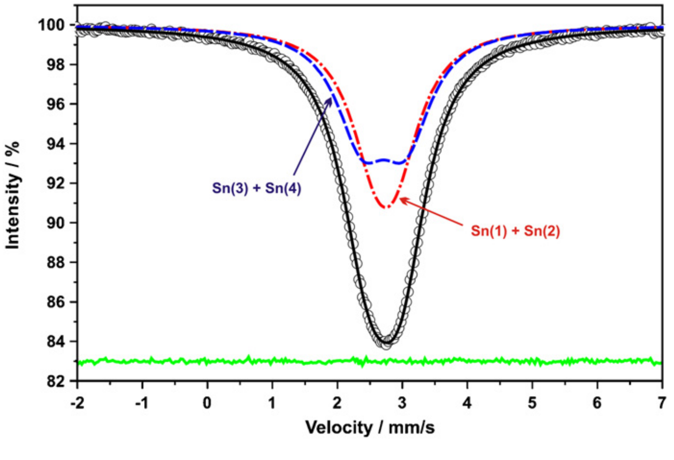

Fig. 4. The ^{119}Sn Mössbauer spectrum of Sn_4As_3 measured at $T = 293$ K. Experimental spectrum, fitted components contributions and the difference curve are shown.

Table 5
Hyperfine parameters of the ^{119}Sn Mössbauer spectrum of Sn_4As_3 obtained at room temperature.

Position	δ (mm/s)	$\varDelta$ (mm/s)	$\varGamma_{1/2}$ (mm/s)	A (%)
Sn(1)+Sn(2)	2.71(1)	0.32(1)	0.95(1)^a	50^b
Sn(3)+Sn(4)	2.68(1)	0.67(1)	0.95(1)^a	50^b

[a] Constrained as equal for both components.
[b] Fixed.

The same approach, unfortunately, cannot be applied to the Sn(1) and Sn(2) atoms, because they possess a slightly distorted octahedral coordination. In this case, the contribution of the 4*d* electrons (the formal sp^3d^2 hybridization) into the electric field gradient and the isomer shift should be taken into account, which

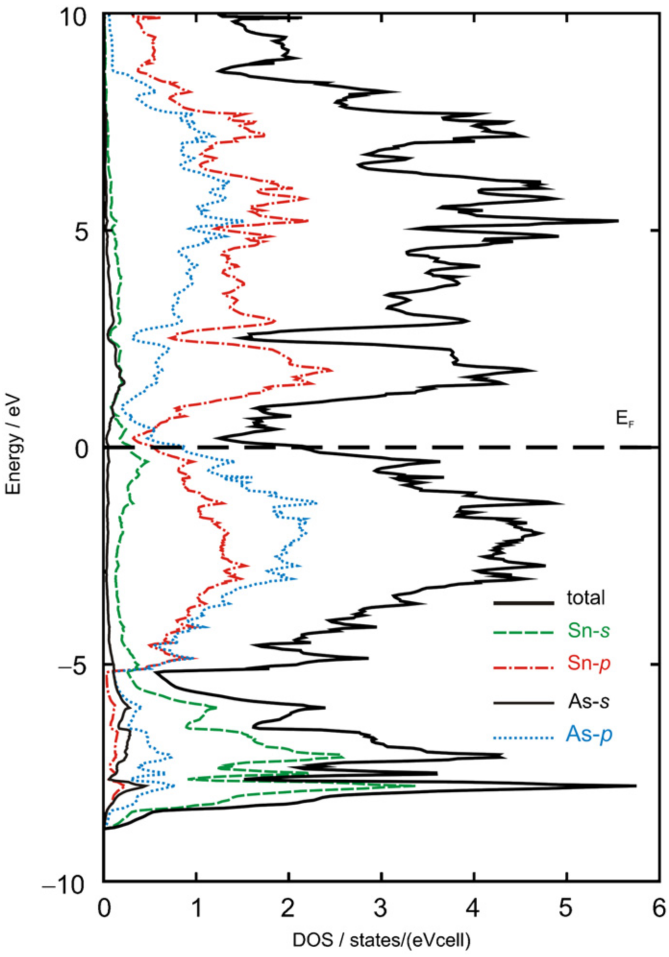

Fig. 5. Density of states (DOS) plot and projections on atomic orbitals for Sn_4As_3.

is practically hard to realize. Therefore, more qualitative analysis was performed. It is noticeable that the minor deviation from the octahedral coordination for the Sn(1) and Sn(2) atoms correlate well with the very low value of the quadrupole splitting, which corresponds to the nearly isotropic electron distribution around the Sn nuclei. The value of the isomer shift is close to that of the β-form of elemental tin ($\delta = 2.65\,\mathrm{mm\,s^{-1}}$) [37]. In the structure of β-Sn, all tin atoms possess a slightly distorted octahedral environment; also, similar to Sn_4As_3, β-Sn is a metallic conductor. Therefore, comparable hyperfine parameters for the Sn(1) and Sn(2) atoms in Sn_4As_3 and for β-Sn are quite justified.

3.4. Electronic structure and bonding

The band structure plot along the high-symmetry directions of Brillouin zone together with the fat-band analysis for Sn_4As_3 is shown in Fig. 6, while the density of states (DOS) plot together with the orbital projections is represented in Fig. 5. From the DOS and band structure diagrams one can conclude that Sn_4As_3 appears to be metallic, in a good agreement with the reported properties [12,15]. The Fermi level resides ~0.4 eV below a minimum (pseudo-gap) of the DOS. In the valence region from −5 eV to the Fermi level the DOS has significant *p*-contributions of Sn and As with the small admixture of Sn *s*-states. The conduction region is preferentially formed by Sn *p*-states, which seems to be reasonable assuming the charge transfer from more electropositive tin to electronegative arsenic. The states below −5 eV originate essentially from Sn *s*-orbitals.

Fat band diagrams show that the bands cross the Fermi level not only in $\Gamma \rightarrow Z$ (perpendicular to the layers) but also in orthogonal directions and they all are made from Sn-*p* and As-*p* states. One may guess that the gap in the band structure cannot thus be opened by simply decreasing the interlayer interactions by pushing layers further apart from each other. The calculations of the hypothetical Sn_4As_3 crystal structures with the interlayer distances up to 4.6 Å confirm this conclusion.

The chemical bonding is further analyzed by means of the ELF [23] and the results are presented in Figs. 7 and 8. As(1) and As(3) have similar bonding picture—each of them has three ELF

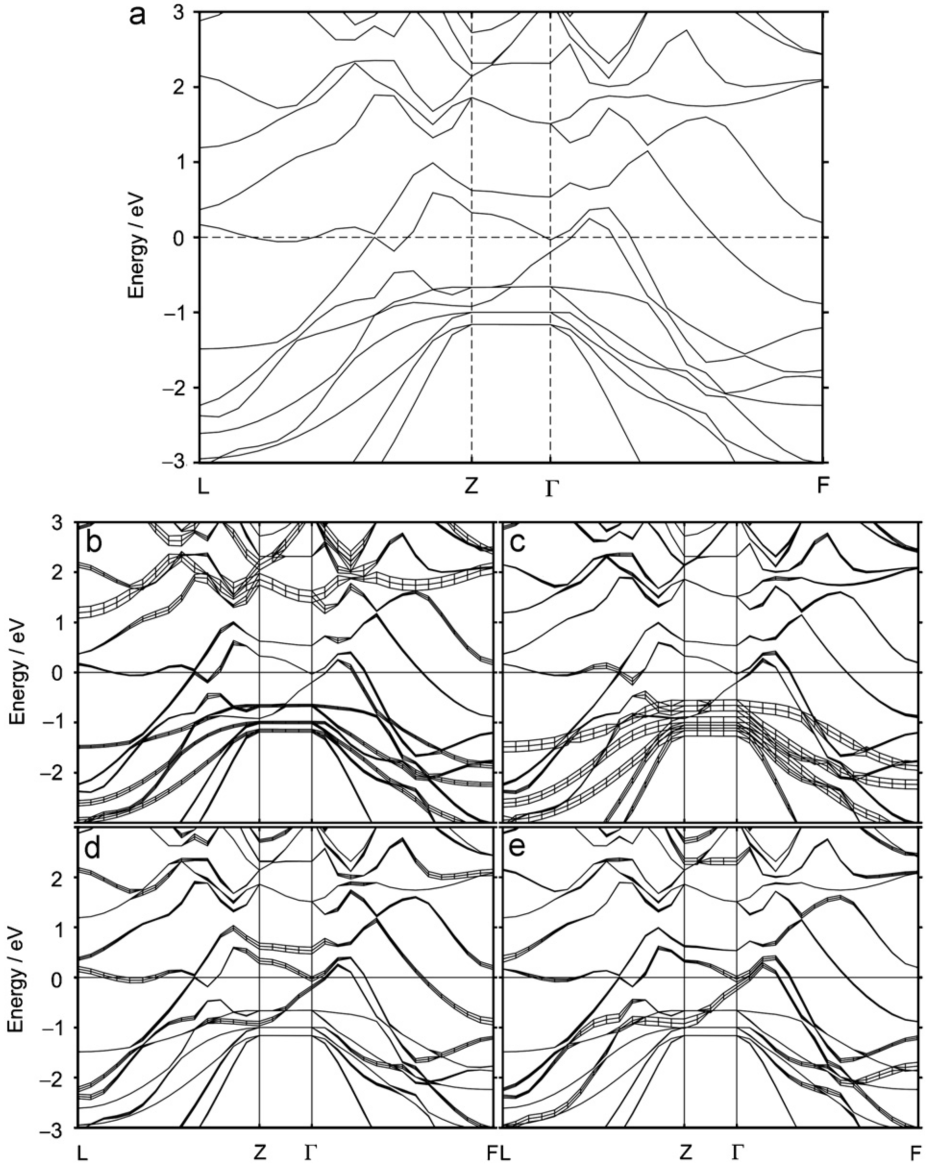

Fig. 6. (a) Band dispersion at the vicinity of Fermi level in Sn_4As_3. Fat band plots with bands drawn with a thickness representative of their corresponding orbital contribution for atomic *p*-orbitals: (b) Sn-p_x and Sn-p_y; (c) As-p_x and As-p_y; (d) Sn-p_z; (e) As-p_z.

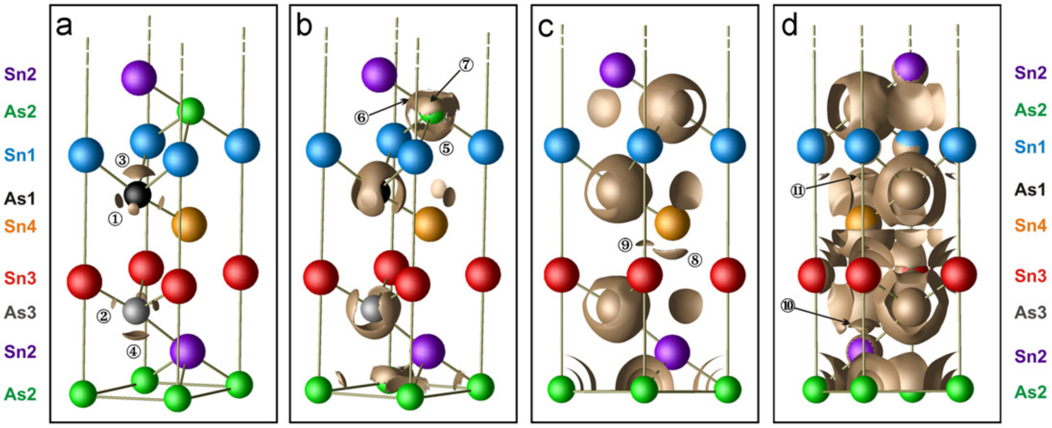

Fig. 7. 3D isosurfaces of electron localization function (η) for Sn_4As_3: (a) $\eta = 0.671$, attractors ① and ② correspond to 2*c* As–Sn interactions, attractors ③ and ④ correspond to 4*c* As+3Sn interactions; (b) $\eta = 0.6435$, bonding around As(2), where 4*c* ⑤, 2*c* ⑥ and 4*c* ⑦ interactions are visible; (c) $\eta = 0.460$, attractors corresponding to lone pairs of Sn(4) ⑧ and Sn(3) ⑨ atoms; (d) $\eta = 0.338$, lone pairs on atoms Sn(2) ⑩ and Sn(1) ⑪.

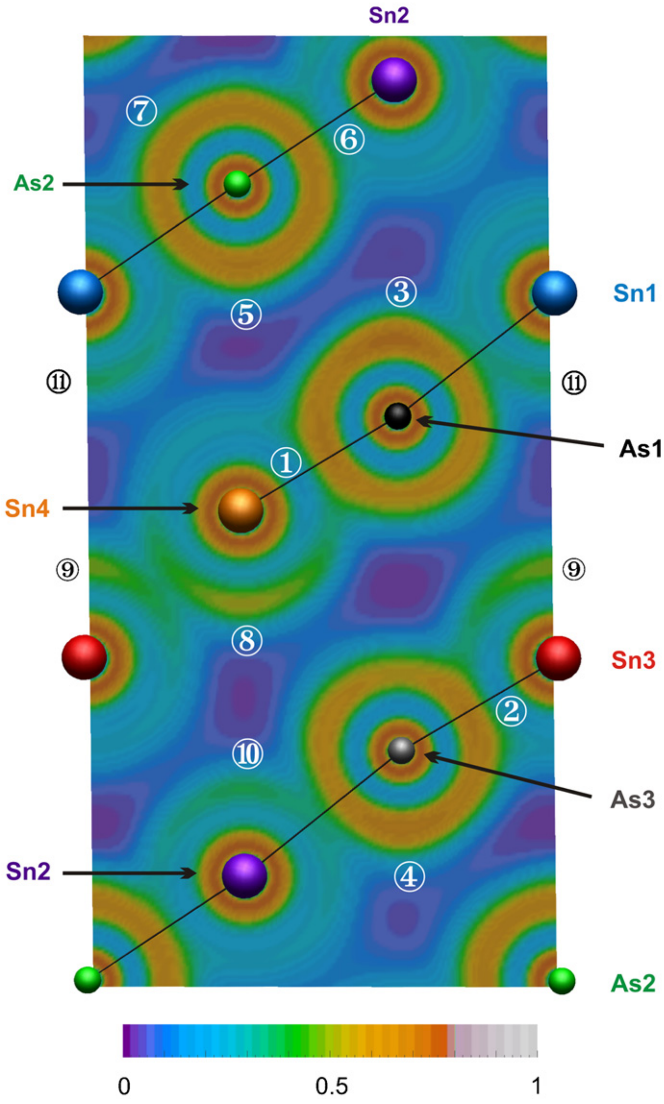

Fig. 8. Coloring of the electron localization function (η) distribution for the slice of the crystal structure of Sn_4As_3 (color bar, below). Attractors are marked with the same symbols as in Fig. 7.

attractors near the As(1)–Sn(4) ① and As(3)–Sn(3) ② interatomic lines corresponding to the shortest interatomic distances in the crystal structure (Fig. 7a). They may be considered as corresponding to the 2*c* As–Sn bonds. Additionally, each of these arsenic atoms has the fourth ELF attractor inside the distorted tetrahedra As(1)+3Sn(1) ③ and As(3)+3Sn(2) ④ with the Sn–As distances about 3.01–3.03 Å (Table 4, Fig. 7a). These attractors may be considered as As lone pairs and can provide the 4*c* interactions between As(1)+3Sn(1) and As(3)+3Sn(2). Thus, As(1) and As(3) have a tetrahedral arrangement of ELF attractors.

Three types of attractors were found around As(2) atoms although some of them are not well resolved (Fig. 7b). Attractor ⑤ in the As(2)+3Sn(1) distorted tetrahedron is most likely a lone pair that can provide the 4*c* interaction As(2)+3Sn(1). Three attractors sit near As(2)–Sn(2) interatomic lines ⑥ and most likely are 2*c* interactions. Finally three ELF attractors ⑦ are also found inside the As(2)+2Sn(2)+Sn(1) distorted tetrahedron. It is reasonable to suggest that they correspond to the 4*c* interaction As(2)+2Sn(2)+Sn(1). Thus, ELF emphasizes the non-centrosymmetric structure of the Sn_4As_3 showing clearly the difference in the As–Sn interactions involving Sn(1) and Sn(2) atoms. Due to the shorter distance to As(2), Sn(2) forms 2*c* and 4*c* bonds while more distant Sn(1) participate only in 4*c* interactions. In case of the centrosymmetric structure these tin atoms should be symmetrically equivalent.

Each Sn(1) atom participates in three 4*c* As(1)+3Sn(1) interactions ③, three 4*c* As(2)+3Sn(1) interactions ⑤, and three 4*c* As(2)+2Sn(2)+Sn(1) interactions ⑦. Additional lone pair attractor is found inside Sn(1)+3As(1) distorted tetrahedron ⑪ (Fig. 7d). Similarly, each Sn(2) participates in three 4*c* As(3)+3Sn(2) interactions ⑥, three 2*c* As(2)–Sn(2) interactions ④, and three 4*c* As(2)+2Sn(2)+Sn(1) interactions ⑦ and also has an additional lone pair attractor ⑩ in the Sn(2)+3As(3) distorted tetrahedron (Fig. 7d).

Atoms Sn(3) and Sn(4) have around them three 2*c* attractors (Sn(3)–As(3) ② and Sn(4)–As(1) ①, correspondingly) and additionally lone pair attractors. In the case of Sn(3) it is located inside the Sn(3)+3Sn(4) tetrahedron ⑨, while lone pair attractor ⑧ for Sn(4) is situated within the Sn(4)+3Sn(3) tetrahedron (Fig. 7c).

In our opinion, the lone pairs of all Sn atoms are not corresponding to any multicenter interactions like the As lone pairs mentioned above but are true lone pairs. The analysis of the

ELF isosurfaces at different levels shows that lone pair isosurfaces are surrounded by the isosurfaces of other lone pairs or 4*c* interaction and most likely cannot come close to other atoms so that the multicenter interaction is impossible. Such isolated lone pairs were already reported for several solid stannides of alkali- and alkali-earth metals [31,32]. It was proposed that repulsive lone pair interactions can lead to the phenomenon of superconductivity in intermetallic compounds [32]. Indeed, superconducting properties were reported for Sn_4As_3 [16].

According to the ELF analysis, two tin atoms, Sn(3) and Sn(4), have classical Sn^{2+} bonding picture—they form three 2*c* bonds and have a lone pair. Two other tin atoms, Sn(1) and Sn(2), participate in multicenter bonding but also have a lone pair each and have similar isomer shifts in Mössbauer spectrum. Thus, all tin atoms can be regarded as Sn^{2+}. In turn, the As(1) and As(3) atoms realize the octet by forming four bonds aligned tetrahedrally (one 4*c* and three 2*c*) and can be regarded as As^{3-}. Electroneutrality of the title compound can be achieved only assuming −2 oxidation state for As(2), i.e. $Sn_4As_3 = (Sn^{2+})_4(As(1)^{3-}As(3)^{3-}As(2)^{2-})$. This explains why As(2) forms complicated multi-centre bonding—it has not enough electrons for realizing octet. One may expect that electron doping to Sn_4As_3 should lead to the formation of Zintl compound which is expected to be a semiconductor. This assumption is in good agreement with formation of pseudo-gap in the conduction band (Fig. 6). According to integration of the DOS, 0.6 electrons are necessary to shift the Fermi level to the pseudo-gap. This can be achieved by partial substitution of tin atoms by arsenic atoms, *viz.* forming $Sn_{4-x}As_{3+x}$, since arsenic has one additional valence electron compared to tin. Thus, the formation of arsenic-rich part of homogeneity range can be explained from the chemical bonding point of view.

4. Conclusions

We have demonstrated that Sn_4As_3 can be produced by solvothermal reaction starting form such simple reagents as metallic tin and elemental arsenic. Presence of ammonia chloride was necessary to get high yields of the reaction. The crystal structure of the title tin arsenide was re-determined and absence of the inversion center was clearly demonstrated by single crystal X-ray analysis. No evidences for either vacancy presence or mixed occupancy of atomic positions were deduced. Detailed analysis of the electronic structure showed that Sn_4As_3 should exhibit metallic properties. Complicated multicenter bonding as well as the presence of lone pairs on the tin atoms were revealed by ELF and Mössbauer spectroscopy.

Acknowledgments

Yu.V.K. thanks JSPS Postdoctoral Fellowships for Foreign Researchers. A.V.So. and A.V.Sh. acknowledge the support of the Russian Foundation for Basic Research.

Appendix A. Supplementary data

Supplementary data associated with this article can be found in the online version at 10.1016/j.jssc.2008.12.007.

References

[1] B.G. Streetman, Solid State Electronic Devices, third ed., Prentice Hall, Englewood Cliffs, NJ, 1990.

[2] [a] J.V. Zaikina, K.A. Kovnir, A.N. Sobolev, I.A. Presniakov, V.G. Kytin, V.A. Kulbachinskii, A.V. Olenev, O.I. Lebedev, G. Van Tendeloo, E.V. Dikarev, A.V. Shevelkov, Chem. Mater. 20 (2008) 2476–2483;
[b] J. Nylén, M. Andersson, S. Lidin, U. Häussermann, J. Am. Chem. Soc. 126 (2004) 16306–16307;
[c] B.C. Sales, D. Mandrus, R.K. Williams, Science 272 (1996) 1325–1328.

[3] [a] F. Gillot, S. Boyanov, L. Dupont, M.-L. Doublet, M. Morcrette, L. Monconduit, J.-M. Tarascon, Chem. Mater. 17 (2005) 6327–6337;
[b] W.C. Zhou, H.X. Yang, S.Y. Shao, X.P. Ai, Y.L. Cao, Electrochem. Commun. 8 (2006) 55–59.

[4] [a] S.T. Oyama, J. Catal. 216 (2003) 343–352
[b] R.L. Halm, K.M. Chadwick, B.R. Keyes, US Patent 4 946 980, 1990.

[5] O. Savadogo, Sol. Energy Mater. Sol. Cells 52 (1998) 361–388.

[6] H.J. Goldsmid, M.E. Ertl, A.J. Dixon, J. Phys. D. 7 (1974) 131–142.

[7] [a] K. Sasma, B. Lv, B. Lorenz, A.M. Guloy, F. Chen, Y. Xue, C. Chu, Phys. Rev. Lett. 101 (2008) 107007;
[b] M. Rotter, M. Tegel, D. Johrendt, Phys. Rev. Lett. 101 (2008) 107006;
[c] N. Ni, S.L. Bud'ko, A. Kreyssig, S. Nandi, G.E. Rustan, A.I. Goldman, S. Gupta, J.D. Corbett, A. Kracher, P.C. Canfield, Phys. Rev. B 78 (2008) 014507;
[d] J.H. Tapp, Z. Tang, B. Lv, K. Sasmal, B. Lorenz, P.C.W. Chu, A.M. Guloy, Phys. Rev. B 78 (2008) 060505.

[8] [a] A.H. Cowley, R.A. Jones, Angew. Chem. Int. Ed. 28 (1989) 1208–1215;
[b] M.A. Olshavsky, A.N. Goldstein, A.P. Alivisatos, J. Am. Chem. Soc. 112 (1990) 9438–9439;
[c] S.S. Kher, R.L. Wells, Chem. Mater. 6 (1994) 2056–2062;
[d] T.J. Trentler, K.M. Hickman, S.C. Goel, A.M. Viano, P.C. Gibbons, W.E. Buhro, Science 270 (1995) 1791–1794.

[9] [a] Y.-D. Li, X.-F. Duan, Y.-T. Qian, L. Yang, M.-R. Ji, C.-W. Li, J. Am. Chem. Soc. 119 (1997) 7869–7870;
[b] Y. Xie, P. Yan, J. Lu, W. Wang, Y. Qian, Chem. Mater. 11 (1999) 2619–2622;
[c] J. Lu, S. Wei, W. Yu, H. Zhang, Y. Qian, Inorg. Chem. 43 (2004) 4543–4545;
[d] S. Wei, J. Lu, W. Yu, H. Zhang, Y. Qian, Inorg. Chem. 44 (2005) 3844–3849;
[e] S. Wei, J. Lu, W. Yu, H. Zhang, Y. Qian, Cryst. Growth Des. 6 (2006) 849–853.

[10] Q.A. Mansuri, J. Chem. Soc. 123 (1923) 214–223.

[11] G. Hägg, A.G. Hybinette, Philos. Mag. 20 (1935) 913–929.

[12] P. Eckerlin, W. Kischio, Z. Anorg. Allg. Chem. 363 (1968) 1–9.

[13] E.A. Peretti, J.K. Paulsen, J. Less-Common Met. 17 (1969) 283–290.

[14] T.Z. Vdovina, Z.S. Medvedeva, Zhurn. Neorg. Khim. 19 (1974) 2257–2260.

[15] Ya.A. Ugai, Yu.P. Zavalskii, V.A. Ugai, S.A. Mostovaya, L.A. Bityuckaya, Dokl. Akad. Nauk SSSR. 163 (1965) 663–666.

[16] [a] S. Geller, G.W. Hull, Phys. Rev. Lett. 13 (1964) 127–129;
[b] M.H. van Marren, Phys. Lett. 29A (1969) 293–294.

[17] L.G. Akselrud, P.Y. Zavalij, Yu. Grin, V.K. Pecharsky, B. Baumgarthner, E. Wölfel, Mater. Sci. Forum 133–136 (1993) 335–337.

[18] V. Petricek, M. Dusek, L, Palatinus. JANA 2000, Institute of Physics, Academy of Science of the Czech Republic, Prague, Czech Republic, 2002.

[19] G.M. Sheldrick, Acta Crystallogr. A 64 (2008) 112–122.

[20] O. Jepsen, A. Burkhardt, O.K. Andersen, The Program TB-LMTO-ASA. Version 4.7, Max-Planck-Institut für Festkörperforschung, Stuttgart, 1999.

[21] U. Barth, L. Hedin, J. Phys. C 5 (1972) 1629–1642.

[22] O.K. Andersen, Phys. Rev. B 12 (1975) 3060–3083.

[23] [a] A.D. Becke, K.E. Edgecombe, J. Chem. Phys. 92 (1990) 5397–5403;
[b] A. Savin, O. Jepsen, J. Flad, O.K. Andersen, H. Preuss, H.G. von Schnering, Angew. Chem. Int. Ed. 31 (1992) 187–188.

[24] IBM's Open Visualization Data Explorer, Version 4.4.4 〈http://www.opendx.org〉.

[25] K.A. Kovnir, Yu.V. Kolen'ko, S. Ray, J. Li, T. Watanabe, M. Itoh, M. Yoshimura, A.V. Shevelkov, J. Solid State Chem. 179 (2006) 3756–3762.

[26] [a] O. Olofsson, Acta Chem. Scand. 24 (1970) 1153–1162;
[b] Y.B. Kuz'ma, S.I. Chikhrii, V.N. Davydov, Inorg. Mater. 35 (1999) 10–11.

[27] [a] S.F. Marenkin, V.M. Trukhan, K.K. Palkina, L.I. Gurskii, T.V. Golyakevich, S.G. Mikhailov, A.V. Molchanov, Zhurn. Neorg. Khim. 51 (2006) 856–859;
[b] A. Continenza, S. Massidda, A.J. Freeman, T.M. de Pascale, F. Meloni, M. Serra, Phys. Rev. B 46 (1992) 10070–10077.

[28] [a] J. Klein, B. Eisenmann, Mater. Res. Bull. 23 (1988) 587–594;
[b] M. Asbrand, B. Eisenmann, J. Klein, Z. Anorg. Allg. Chem. 621 (1995) 576–582;
[c] B. Eisenmann, U. Rößler, Z. Anorg. Allg. Chem. 626 (2000) 1373–1379.

[29] [a] K.A. Kovnir, A.V. Sobolev, I.A. Presniakov, O.I. Lebedev, G. Van Tendeloo, W. Schnelle, Yu. Grin, A.V. Shevelkov, Inorg. Chem. 44 (2005) 8786–8793;
[b] J.V. Zaikina, K.A. Kovnir, A.V. Sobolev, I.A. Presniakov, Yu. Prots, M. Baitinger, W. Schnelle, A.V. Olenev, O.I. Lebedev, G. Van Tendeloo, Yu. Grin, A.V. Shevelkov, Chem. Eur. J. 13 (2007) 5090–5099.

[30] J.J. Gulman, Solid State Chem. 87 (1990) 202–207.

[31] [a] T.F. Fässler, S. Hoffmann, Z. Anorg. Allg. Chem. 626 (2000) 106–112;
[b] S. Hoffmann, T.F. Fässler, Inorg. Chem. 42 (2003) 8748–8754.

[32] T.F. Fässler, Chem. Soc. Rev. 32 (2003) 80–86.

[33] [a] H.G. von Schnering, R. Kröner, M. Baitinger, K. Peters, R. Nesper, Yu. Grin, Z. Kristallogr. NCS 215 (2000) 205;
[b] F. Dubois, T.F. Fässler, J. Am. Chem. Soc. 127 (2005) 3264–3265;
[c] A. Kaltzoglou, S.D. Hoffmann, T.F. Fässler, Eur. J. Inorg. Chem. (2007) 4162–4167.

[34] [a] M.M. Shatruk, K.A. Kovnir, A.V. Shevelkov, I.A. Presniakov, B.A. Popovkin, Inorg. Chem. 38 (1999) 3455–3457;
[b] K.A. Kovnir, J.V. Zaikina, L.N. Reshetova, A.V. Olenev, E.V. Dikarev, A.V. Shevelkov, Inorg. Chem. 43 (2004) 3230–3236;
[c] J.V. Zaikina, W. Schnelle, K.A. Kovnir, A.V. Olenev, Yu. Grin, A.V. Shevelkov, Solid State Sci. 9 (2007) 664–671.
[35] C.H. Townes, B.P.J. Dailey, Chem. Phys. 17 (1949) 782–799.
[36] M.M. Shatruk, K.A. Kovnir, M. Lindsjö, I.A. Presniakov, L.A. Kloo, A.V. Shevelkov, J. Solid State Chem. 161 (2001) 233–242.
[37] P.A. Flinn, in: G.K. Shenoy, F.E. Wagner (Eds.), Mossbauer Isomer Shifts, North Holland, Amsterdam, 1978, p. 593.